ELSEVIER

Comput. Methods Appl. Mech. Engrg. 190 (2000) 1701–1718

Computer methods in applied mechanics and engineering

www.elsevier.com/locate/cma

Locking-free adaptive mixed finite element methods in linear elasticity

C. Carstensen [a], G. Dolzmann [b], S.A. Funken [a,*], D.S. Helm [a]

[a] *Mathematisches Seminar, Christian-Albrechts-Universität zu Kiel, Ludewig-Meyn-Str. 4, D-24098 Kiel, Germany*

[b] *Max Planck Institute for Mathematics in the Sciences, Inselstr. 22-26, D-04103 Leipzig, Germany*

Received 8 July 1998; received in revised form 8 July 1999

Dedicated to D. Braess

Abstract

Mixed finite element methods such as PEERS or the BDMS methods are designed to avoid locking for nearly incompressible materials in plane elasticity. In this paper, we establish a robust adaptive mesh-refining algorithm that is rigorously based on a reliable and efficient a posteriori error estimate. Numerical evidence is provided for the λ-independence of the constants in the a posteriori error bounds and for the efficiency of the adaptive mesh-refining algorithm proposed. © 2000 Elsevier Science B.V. All rights reserved.

Keywords: A posteriori error estimates; Adaptive algorithm; Reliability; Mixed finite element method; Locking

1. Introduction

In this paper we investigate finite element solutions of the Lamé system in linear elasticity and consider a plane elastic body with reference configuration $\Omega \subset \mathbb{R}^2$ and boundary $\partial\Omega = \Gamma = \Gamma_D \cup \Gamma_N$, $\Gamma_D \neq \emptyset$, $\Gamma_N = \Gamma \setminus \Gamma_D$. Given a volume force $f : \Omega \to \mathbb{R}^2$ and a traction $g : \Gamma_N \to \mathbb{R}^2$, we seek (an approximation to) the displacement field $u : \Omega \to \mathbb{R}^2$ and the stress tensor $\sigma : \Omega \to M^{2\times 2}_{\mathrm{sym}} := \{\tau \in \mathbb{R}^{2\times 2} : \tau = \tau^{\mathrm{t}}\}$ satisfying

$$-\operatorname{div}\sigma = f, \tag{1.1}$$
$$\sigma = \mathbb{C}\varepsilon(u) \quad \text{in } \Omega, \tag{1.2}$$
$$u = 0 \quad \text{on } \Gamma_D, \tag{1.3}$$
$$\sigma n = g \quad \text{on } \Gamma_N, \tag{1.4}$$

where $\varepsilon(v) = \frac{1}{2}(\nabla v + (\nabla v)^{\mathrm{t}})$ is the linearized Green strain tensor and

$$\sigma = \lambda\,\mathrm{tr}(\varepsilon(u))\mathrm{Id} + 2\mu\varepsilon(u) \tag{1.5}$$

is the Cauchy stress tensor (under the plain strain hypothesis). For positive Lamé constants λ and μ, the fourth-order elasticity tensor $\mathbb{C}$ is symmetric, bounded, and positive definite; $\mathrm{tr}(A) = A_{11} + A_{22}$ is the trace of the matrix A and Id is the 2×2 unit matrix. As a consequence of Korn's inequality and the Lax–Milgram lemma, Problem (1.1)–(1.4) has a unique solution $(\sigma, u) \in L^2(\Omega; M^{2\times 2}_{\mathrm{sym}}) \times H^1(\Omega)^2$.

* Corresponding author.

E-mail addresses: cc@numerik.uni-kiel.de (C. Carstensen), georg@mis.mpg.de (G. Dolzmann), saf@numerik.uni-kiel.de (S.A. Funken), dsh@numerik.uni-kiel.de (D.S. Helm).

PII: S 0 0 4 5 - 7 8 2 5 (0 0) 0 0 1 8 5 - 7

For nearly incompressible materials, i.e., for a Poisson ration ν near to $1/2$, the Lamé constant λ is very large and the standard computation of a finite element solution u_h which is based on a displacement formulation (where (1.5) is used to substitute σ in (1.1) and (1.4)) fails: The constant $C(\lambda)$ in the error estimate

$$||\mathbb{C}^{1/2}\varepsilon(u-u_h)||2,\Omega \leqslant C(\lambda)h^{\alpha} \tag{1.6}$$

(for small mesh-sizes h) tends to infinity as $\lambda \to \infty$. To illustrate this locking effect, Fig. 1 displays the energy error vs mesh-size of numerical results for six sequences of uniform meshes with six different Poisson ratios ν. For each ν, an entry $*$ is given at the position $(\sqrt{N},\ ||\ \mathbb{C}^{1/2}\varepsilon(u-u_h)\ ||_{2,\Omega})$ for a mesh with N degrees of freedoms. The description of the underlying test example will be given below in Section 6. Note that we have a logarithmic scaling on both axes and so we observe from Fig. 1 that the empirical convergence rate α is approximately 0.5445 which is the (negative) slope of the affine interpolation of the data points. This is in agreement with theoretical predictions because the exact solution has a singularity at the re-entering corner of the domain Ω. The dependence of the constant in (1.6) suggests $C(\lambda) \propto 1/(0.5-\nu) \propto \lambda$: Multiplication of λ by 10 increases the error by a factor $3.16 \approx \sqrt{10}$.

Mixed finite element formulations are designed for a robust approximation, i.e., the constant $C(\lambda)$ in an error estimate as (1.6) is then λ-independent. Stable numerical schemes are obtained by relaxing the symmetry of the discrete stress tensor σ_h [3,8,19,21]: We seek (an approximation to) $u:\Omega\to\mathbb{R}^2$, $\sigma:\Omega\to\mathbb{R}^{2\times 2}$ and $\gamma:\Omega\to M^{2\times 2}_{\text{skew}} := \{\eta\in\mathbb{R}^{2\times 2} : \eta+\eta^{\mathrm{t}}=0\}$ satisfying

$$\sigma=\mathbb{C}(\nabla u-\gamma),\quad \sigma=\sigma^{\mathrm{t}},\quad -\operatorname{div}\sigma=f \ \text{ in } \Omega,\quad u=0 \ \text{ on } \Gamma_D,\quad \sigma n=g \ \text{ on } \Gamma_N. \tag{1.7}$$

We refer to Section 2 for a variational formulation and its discretization which yields the approximation $(\sigma_h,u_h,\gamma_h)\in\Sigma_{g,h}\times\mathscr{U}_h\times\mathscr{W}_h$ with respect to PEERS (plane elasticity element with reduced symmetry) [3] and a modification of the BDM element BDM_k due to Stenberg which we will therefore refer to as BDMS_k element.

The practical performance of the PEERS is robust in the sense that, at least for very small mesh-sizes, the error is (almost) independent of the crucial parameter $\nu\to 1/2$. This is supported by Fig. 2 where we display numerical results for the lowest order PEERS in Example 6.1 (compare with Fig. 1).

In the example, a corner singularity reduces the convergence rate from the optimal value 1 to $\alpha=0.5445$. This paper aims to improve such a poor convergence rate by proposing a robust mesh-refining algorithm for an efficient automatic mesh-design. In contrast to the ansatz in [6], our algorithm is rigorously based on an efficient and reliable a posteriori error estimate in natural norms established in [12] and proved with methods from [2,10].

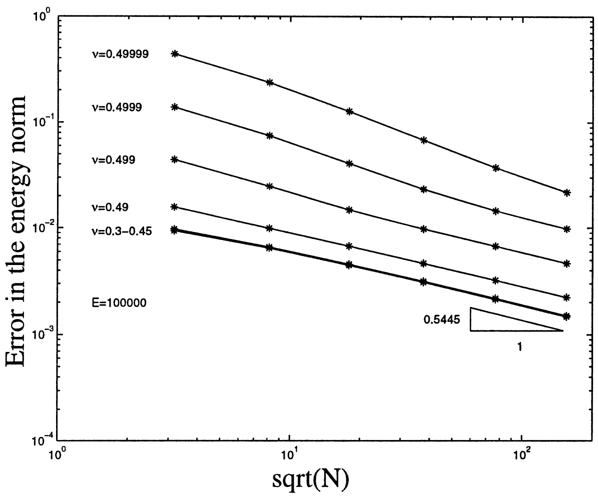

Fig. 1. Energy norm of P_1-displacement FE approximation error on the uniform mesh in Example 6.1 vs degrees of freedom N.

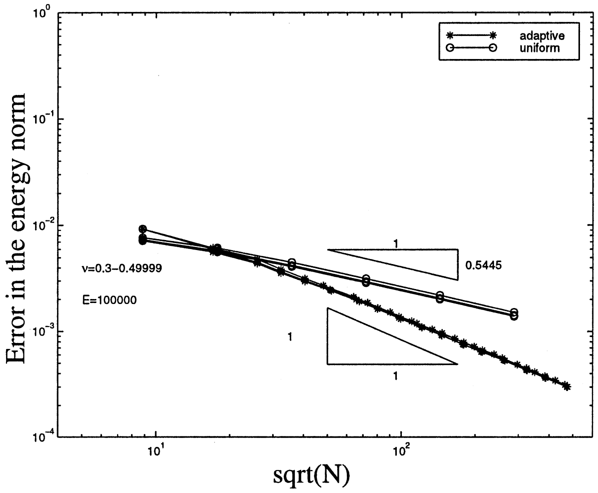

Fig. 2. PEERS approximation error on uniform and adaptive meshes in Example 6.1 vs degrees of freedom (energy norm of the stress errors).

Given the discrete solution $(\sigma_h, u_h, \gamma_h)$ and an element T in the triangulation $\mathscr{T}_h$, we compute

$$\eta_T^2 := \frac{h_T^2}{\mu^2}\|f + \operatorname{div}\sigma_h\|_{2;T}^2 + h_T^2\|\operatorname{curl}(\mathbb{C}^{-1}\sigma_h + \gamma_h)\|_{2;T}^2 + \frac{1}{\mu^2}\|\operatorname{As}(\sigma_h)\|_{2;T}^2 \\ + h_E\|\left[(\mathbb{C}^{-1}\sigma_h + \gamma_h)t_E\right]\|_{2;\partial T\setminus\Gamma}^2 + h_E\|g - \sigma_h n\|_{2;\partial T\cap\Gamma_N}^2 + h_E\|\left[(\mathbb{C}^{-1}\sigma_h + \gamma_h - \nabla u_D)t_E\right]\|_{2;\partial T\cap\Gamma_D}^2. \quad (1.8)$$

Here, h_T is the diameter of T and E is an edge of T with length h_E and $[\cdot]$ denotes the jump of the indicated quantity over an inner-element edge E. (See Section 3 for a detailed notation.) Notice that all terms are residuals: $f + \operatorname{div}\sigma_h$ is the residual of (1.1), $\operatorname{curl}(\mathbb{C}^{-1}\sigma_h + \gamma_h)$ and $\left[(\mathbb{C}^{-1}\sigma_h + \gamma_h)t_E\right]$ are residuals of $\mathbb{C}^{-1}\sigma + \gamma = \nabla u$ (since the $\operatorname{curl}\nabla u = 0$ and $\partial u/\partial s = \nabla u \cdot t_E = 0$), $\operatorname{As}(\sigma_h)$ is the residual to $\operatorname{As}\sigma = 0$, and the remaining terms are their modifications on the boundary of the domain. Then the proposed mesh-refining algorithm generates a sequence of meshes and related Galerkin solutions. The corresponding errors are shown in Fig. 2.

Adaptive algorithm (A)

(a) Start with coarse mesh $\mathscr{T}_0$.
(b) Solve discrete problem w.r.t. $\mathscr{T}_k$.
(c) Compute η_T for all $T \in \mathscr{T}_k$.
(d) Compute error bound $\left(\sum_{T\in\mathscr{T}_k}\eta(T)^2\right)^{1/2}$ and terminate or goto (e).
(e) Mark element T red iff $\eta(T) \geqslant \frac{1}{2}\max_{T'\in\mathscr{T}_k}\eta(T')$.
(f) Perform red–green–blue-refinement to avoid hanging nodes, update mesh and goto (b).

We refer to [4,18,23] for details on red–green–blue refinement procedures and corresponding data handling.From the numerical results in Fig. 2, we conclude that our algorithm is efficient (because the experimental convergence rate is improved to the optimal value 1) and robust (because the errors are almost independent of $\lambda \to \infty$).

The remaining part of the paper is organized as follows. The discrete subspaces as well as the weak form to (1.7) are described in Section 2. The underlying a posteriori error estimate is given in Section 3. The proof is given in Section 4 for convenient reading and because, compared to [12], we use different scalings with the Lamé constant μ. This leads to an a posteriori estimate

$$||\mathbb{C}^{1/2}(\sigma - \sigma_h)||2, \Omega \leqslant c_1\left(\sum_{T\in\mathscr{T}_h}\eta_T^2\right)^{1/2} =: c_1\eta(\sigma;\mathscr{T}_h), \quad (1.9)$$

where the constant c_1 is independent of λ and μ. Since PEERS appears to be not very frequently used in practice, we give some details of our realization in Section 5. The experimental results are presented and discussed in Section 6. In particular, we will see that the convergence behavior in Example 6.1 can indeed be optimized by Algorithm (A).

2. Mixed finite elements

In the mixed variational formulation one seeks $(\sigma, u, \gamma) \in \Sigma_g \times \mathcal{U} \times \mathcal{W}$ such that

$$a(\sigma, \tau) + b(\tau; u, \gamma) = 0 \quad \text{and} \quad b(\sigma; v, \eta) = -(f, v) \tag{2.1}$$

for all $(\tau, v, \eta) \in \Sigma_0 \times \mathcal{U} \times \mathcal{W}$. Here, the linear and bilinear forms and the function spaces Σ_t, $\mathcal{U}$, $\mathcal{W}$ are defined for $t = 0$ and $t = g$ by

$$\begin{aligned}
a(\sigma, \tau) &= \int_\Omega \mathbb{C}^{-1}\sigma : \tau \, dx, \\
b(\sigma; u, \gamma) &= \int_\Omega (u \cdot \operatorname{div}\sigma + \sigma : \gamma) \, dx, \\
(f, v) &= \int_\Omega f \cdot v \, dx, \\
\Sigma_t &= \{\sigma \in L^2(\Omega; \mathbb{R}^{2\times 2}) : \operatorname{div}\sigma \in L^2(\Omega; \mathbb{R}^2), \ \sigma n = t \text{ on } \Gamma_N\}, \\
\mathcal{U} \times \mathcal{W} &= L^2(\Omega; \mathbb{R}^2) \times L^2(\Omega; M^{2\times 2}_{\text{skew}}).
\end{aligned}$$

In this approach, the symmetry of the stress tensor σ is relaxed and only imposed by means of the Lagrange multiplier γ. For $\Sigma_{t,h}$, $\mathcal{U}_h$, $\mathcal{W}_h$ finite dimensional spaces approximating Σ_t, $\mathcal{U}$, and $\mathcal{W}$ we define the discrete solution $(\sigma_h, u_h, \gamma_h) \in \Sigma_{g,h} \times \mathcal{U}_h \times \mathcal{W}_h$ by

$$a(\sigma_h, \tau_h) + b(\tau_h; u_h, \gamma_h) = 0 \quad \text{and} \quad b(\sigma_h; v_h, \eta_h) = -(f, v_h) \tag{2.2}$$

for all $(\tau_h, v_h, \eta_h) \in \Sigma_{0,h} \times \mathcal{U}_h \times \mathcal{W}_h$. In this formulation, σ_h satisfies only the weak symmetry condition, i.e., for all $\gamma_h \in \mathcal{W}_h$,

$$\int_\Omega \sigma_h : \gamma_h \, dx = 0, \tag{2.3}$$

which does not imply $\sigma_h = \sigma_h^{\mathrm{t}}$ if $\sigma_h - \sigma_h^{\mathrm{t}} \notin \mathcal{W}_h$. In two dimensions, existence, uniqueness, and a priori estimates for several choices of discrete spaces have been proven in [21] which include the low order PEERS (plane elasticity element with reduced symmetry) constructed by Arnold et al. [3] and a modification of the Brezzi–Douglas–Marini element BDM_k due to Stenberg (which we will refer to as BDMS_k element).

We assume that Ω is a simply connected bounded domain in $\mathbb{R}^2$ with polygonal boundary. Let $\mathcal{T}_h$ be a regular triangulation of Ω in the sense of Ciarlet [17], which satisfies the minimum angle condition, i.e., there exists a constant $c_2 > 0$ such that $c_2^{-1} h_T^2 \leqslant |T| \leqslant c_2 h_T^2$. Here, $|T|$ is the area and h_T is the diameter of $T \in \mathcal{T}_h$. The set of all element sides in $\mathcal{T}_h$ is denoted by $\mathcal{E}_h$ and h_E is the length of the edge $E \in \mathcal{E}_h$. We assume in addition that Γ_N is a finite union of connected components Γ_i, $i = 0, \ldots, M$, and that Γ_D has positive surface measure. Thus we have $\mathcal{E}_h = \mathcal{E}_\Omega \cup \mathcal{E}_D \cup \mathcal{E}_N$ where $\mathcal{E}_\Omega$ is the set of all interior element sides and $\mathcal{E}_D$ and $\mathcal{E}_N$ are the collection of all edges contained in Γ_D and Γ_N, respectively. We write $\mathcal{E}_h^0 = \mathcal{E}_\Omega \cup \mathcal{E}_N$. It is useful to define a function $h_{\mathcal{T}_h}$ on Ω by $h_{\mathcal{T}_h}|_T = h_T$ and a function $h_{\mathcal{E}_h}$ on the union of all element sides by $h_{\mathcal{E}_h}|_E = h_E$.

The definition of the finite element spaces involves the bubble function $b_T = \lambda_1\lambda_2\lambda_3$ on a triangle $T \in \mathcal{T}_h$, where λ_i are the barycentric coordinates on T. The PEERS is based on the following function spaces:

$$\mathscr{U}_h = \{v_h \in \mathscr{U} : \ \forall T \in \mathscr{T}_h \ v_h|_T \in \mathscr{P}_0(T)^2\},$$
$$\mathscr{W}_h = \{\gamma_h \in \mathscr{W} \cap C^0(\Omega; M^{2\times 2}_{\text{skew}}) : \ \forall T \in \mathscr{T}_h \ \gamma_h|_T \in \mathscr{P}_1(T; M^{2\times 2}_{\text{skew}})\},$$
$$\Sigma_h = \{\sigma_h \in L^2(\Omega; M^{2\times 2}) : \ \ \operatorname{div}\sigma_h \in \mathscr{U}, \quad \forall T \in \mathscr{T}_h \ \sigma_h|_T \in RT_0(T) \oplus B_0(T)\},$$
$$\Sigma_{t,h} = \{\sigma_h \in \Sigma_h : \ \sigma_h n = \tilde{t} \text{ on } \Gamma_N\},$$

where $\tilde{t}$ is the $L^2(E)$-projection of t onto $\mathscr{P}_0(E)^2$ for all edges $E \subset \Gamma_N$. Here, RT_0 is the Raviart–Thomas space of lowest degree, and

$$RT_0(T) = \{\sigma \in L^2(T; M^{2\times 2}) : \ \sigma = \tau + a \otimes x, \ \tau \in M^{2\times 2}, a \in \mathbb{R}^2\},$$
$$B_0(T) = \{\sigma \in L^2(T; M^{2\times 2}) : \ \sigma = a \otimes \operatorname{Curl} b_T, \ a \in \mathbb{R}^2\},$$
$$\mathrm{BDM}_k(\Omega) = \{\sigma_h \in L^2(\Omega; M^{2\times 2}) : \ \ \operatorname{div}\sigma_h \in \mathscr{U}, \ \sigma_h|_T \in \mathscr{P}_k(T; M^{2\times 2})\}.$$

The higher order methods BDMS_k are defined for $k \geqslant 2$ by

$$\mathscr{U}_h = \{v_h \in \mathscr{U} : \ \forall T \in \mathscr{T}_h \ v_h|_T \in \mathscr{P}_{k-1}(T)^2\},$$
$$\mathscr{W}_h = \{\gamma_h \in \mathscr{W} : \ \forall T \in \mathscr{T}_h \ \gamma_h|_T \in \mathscr{P}_k(T; M^{2\times 2}_{\text{skew}})\},$$
$$\Sigma_h = \{\sigma_h \in L^2(\Omega; M^{2\times 2}) : \ \ \operatorname{div}\sigma \in \mathscr{U}, \quad \forall T \in \mathscr{T}_h \ \sigma_h|_T \in \mathscr{P}_k(T; M^{2\times 2}) \oplus B_{k-1}(T)\},$$
$$\Sigma_{t,h} = \{\sigma_h \in \Sigma_h : \ \sigma_h n = \tilde{t} \text{ on } \Gamma_N\},$$

where $\tilde{t}$ is the $L^2(E)$-projection of t onto $\mathscr{P}_k(E)^2$, i.e., $\tilde{t}|_E := \int_E t\,\mathrm{d}s/\mathrm{meas}(E)$ if $k = 0$, and

$$B_{k-1}(T) = \{\sigma \in L^2(T; M^{2\times 2}) : \ \sigma = \operatorname{Curl}(b_T w), \ w \in \mathscr{P}_{k-1}(T)^2\}.$$

3. A posteriori error estimate

Let $L^2(\Omega)$ denote the standard Lebesgue space with norm $\|\cdot\|_{2,\Omega}$, $H^1(\Omega)$ the Sobolev space with norm $\|\cdot\|_{1,2,\Omega}$ and seminorm $|\cdot|_{1,2,\Omega}$, and $L^2(\Omega; S) := \{v \in L^2(\Omega) | v : \Omega \to S\}$. We write $u \in L^2(\mathscr{T}_h)$ (resp. $v \in H^1(\mathscr{T}_h)$) and $w \in L^2(\mathscr{E}_h)$ if $u|_T \in L^1(T)$ (resp. $v|_T \in H^1(T)$) for all $T \in \mathscr{T}_h$ and $w|_E \in L^2(E)$ for all $E \in \mathscr{E}_h$. For each $E \in \mathscr{E}_h$ we fix a normal n_E to E such that n_E coincides with the exterior normal to $\partial\Omega$ if $E \subset \partial\Omega$. Then,

$$[v]|_E := (v|_{T^+})|_E - (v|_{T^-})|_E$$

if $E = \bar{T}^+ \cap \bar{T}^-$ and n_E is the exterior normal to T^+ on E and

$$[v]|_E = (v|_T)|_E$$

if $E = \bar{T} \cap \partial\Omega$. Finally we define

$$\operatorname{Curl}\Phi = (\Phi_{,2}, -\Phi_{,1}) \quad \text{for } \Phi \in H^1(\Omega),$$

$$\operatorname{Curl} u = \begin{pmatrix} u_{1,2} & -u_{1,1} \\ u_{2,2} & -u_{2,1} \end{pmatrix}, \quad \operatorname{curl} u = u_{2,1} - u_{1,2},$$

$$\operatorname{curl}\sigma = \begin{pmatrix} \sigma_{12,1} - \sigma_{11,2} \\ \sigma_{22,1} - \sigma_{21,2} \end{pmatrix}, \quad \operatorname{div}\sigma = \begin{pmatrix} \sigma_{11,1} + \sigma_{12,2} \\ \sigma_{21,1} + \sigma_{22,2} \end{pmatrix}.$$

Theorem 3.1. *Let $\mathscr{T}_h$ be a shape-regular triangulation of $\Omega \subset \mathbb{R}^2$ and let $(\sigma_h, u_h, \gamma_h)$ be the solution of* (2.2) *for the* PEERS *or the* BDMS_k *element. Then there exists a λ- and μ-independent constant c_3, which depends only on $\Omega, \Gamma_N, \Gamma_D$ and the polynomial degree of the elements, such that*

$$\|\mathbb{C}^{-1/2}(\sigma - \sigma_h)\|_{2;\Omega} \leqslant c_3 \eta(\sigma; \mathscr{T}_h) := c_3 \left(\sum_{T \in \mathscr{T}_h} \eta_T^2 \right)^{1/2}.$$

Remark 3.1 (*Displacement estimate*). A more general estimate is given in [12]:

$$\|u - u_h\|_{2;\Omega} + \|\gamma - \gamma_h\|_{2;\Omega} + \|\mathbb{C}^{-1/2}(\sigma - \sigma_h)\|_{2;\Omega} \leqslant c_4 \left(\eta(\sigma; \mathscr{T}_h)^2 + \sum_{T \in \mathscr{T}_h} h_T^2 \inf_{v_h \in \mathscr{U}_h} \|\mathbb{C}^{-1}\sigma_h + \gamma_h - \nabla v_h\|_{2;T}^2 \right)^{1/2}. \tag{3.1}$$

Remark 3.2 (*Efficiency*). Assume in addition to the hypotheses of Theorem 3.1 that $\mathrm{curl}(\mathbb{C}^{-1}\sigma_h + \gamma_h)|_T$ is a polynomial for all $T \in \mathscr{T}_h$ and $(\sigma - \sigma_h)n|_E$ for all $E \subset \Gamma_N$. Then there exists a constant c_5, which depends only on Ω, μ, and the polynomial degree of the elements, such that

$$\eta(\sigma; \mathscr{T}_h) \leqslant c_5 \Big(\|u - u_h\|_{2;\Omega} + \|\mathbb{C}^{-1}(\sigma - \sigma_h) + \gamma - \gamma_h\|_{2;\Omega} + \|\sigma - \sigma_h\|_{2;\Omega} + \|h_{\mathscr{T}_h}(f + \mathrm{div}\,\sigma_h)\|_{2;\Omega} \Big).$$

Remark 3.3 (*Volume contributions*). As explained in [11], a Clément-type weak interpolation can be used to refine Theorem 3.1. Indeed, the contribution

$$\sum_{T \in \mathscr{T}_h} h_T^2 \|\mathrm{curl}(\mathbb{C}^{-1}\sigma_h + \gamma_h)\|_{2;T}^2$$

could be replaced by a higher-order term [15].

4. Proof of a posteriori error estimate

The proof is in the spirit of Alonso and Carstensen [2,10,12] and based on a Helmholtz decomposition of $\sigma - \sigma_h = \mathrm{sym}(\sigma - \sigma_h) - \varphi$ where $\mathrm{sym}(\cdot) := \left[(\cdot) + (\cdot)^{\mathrm{t}}\right]/2$ and $\varphi := \mathrm{As}(\sigma_h)$. Define $v \in H_D^1(\Omega) := \{v \in H^1(\Omega)^2 : \ v = 0 \text{ on } \Gamma_D\}$ as the solution to

$$\int_\Omega \varepsilon(w) : \mathbb{C}\varepsilon(v)\,\mathrm{d}x = \int_\Omega \varepsilon(w) : \ (\sigma - \sigma_h)\,\mathrm{d}x \quad (w \in H_D^1(\Omega)). \tag{4.1}$$

Then, $S := \sigma - \sigma_h - \mathbb{C}\varepsilon(v) + \varphi \in L^2(\Omega; M_{\mathrm{sym}}^{2\times 2})$ satisfies

$$\int_\Omega S : \nabla w\,\mathrm{d}x = 0 \quad (w \in H_D^1(\Omega)) \tag{4.2}$$

and so, for $j = 1, 2$, (S_{j1}, S_{j2}) is divergence-free. According to classical results in potential theory, (S_{j1}, S_{j2}) is some $\mathrm{Curl}\,\psi_j$, i.e., $S = \mathrm{Curl}\,\psi$ for some $\psi \in H^1(\Omega)^2$. We refer to [20,22] for details. Partial integration of (4.2) shows $\int_{\Gamma_N} w \cdot Sn\,\mathrm{d}s = 0$. Since w is arbitrary on Γ_N, $Sn = 0$, whence $\mathrm{Curl}\,\psi n = 0$ with $t = (-n_2, n_1)$. This is $\nabla\psi \cdot t = 0$, i.e., ψ is constant on each component of Γ_N. Because $S = \mathrm{Curl}\,\psi$ is symmetric, $\psi_{1,1} + \psi_{2,2} = 0$ and so ψ is divergence-free. Thus, $\psi = \mathrm{Curl}\,\Phi$ for some $\Phi \in H^2(\Omega)$. Altogether, cf. [12, Section 3],

$$\sigma - \sigma_h = \mathbb{C}\varepsilon(v) + \mathrm{Curl}\,\mathrm{Curl}\,\Phi - \varphi, \quad \text{where } \varphi = \mathrm{As}(\sigma_h).$$

Therefore, the stress error is decomposed as

$$\int_\Omega \mathbb{C}^{-1}(\sigma-\sigma_h):(\sigma-\sigma_h)\,\mathrm{d}x = \int_\Omega \varepsilon(v):(\sigma-\sigma_h)\,\mathrm{d}x + \int_\Omega \operatorname{Curl}\operatorname{Curl}\Phi:\mathbb{C}^{-1}(\sigma-\sigma_h)\,\mathrm{d}x - \int_\Omega \varphi:\mathbb{C}^{-1}(\sigma-\sigma_h)\,\mathrm{d}x \tag{4.3}$$

and we have

$$\|\mathbb{C}^{-1/2}(\sigma-\sigma_h)\|_{2;\Omega} \leqslant \|\mathbb{C}^{-1/2}\operatorname{Curl}\operatorname{Curl}\Phi\|_{2;\Omega} + \|\mathbb{C}^{1/2}\varepsilon(v)\|_{2;\Omega} + \|\mathbb{C}^{-1/2}\varphi\|_{2;\Omega}. \tag{4.4}$$

Since $\mathbb{C}^{-1}\sigma = \varepsilon(u)$ and since $\operatorname{Curl}\operatorname{Curl}\Phi$ is symmetric we have

$$\int_\Omega \operatorname{Curl}\operatorname{Curl}\Phi:\mathbb{C}^{-1}(\sigma-\sigma_h)\,\mathrm{d}x = \int_\Omega \operatorname{Curl}\operatorname{Curl}\Phi:(\nabla u - \mathbb{C}^{-1}\sigma_h)\,\mathrm{d}x. \tag{4.5}$$

Let $\Psi \in \mathscr{S}^1(\mathscr{T}_h)$ be constant on each component of Γ_N and equal to ψ there. The assumption on the trial space is $\tau_h := \operatorname{Curl}\Psi \in \Sigma_{0,h}$ and so $\operatorname{div}\tau_h = 0$ and (2.2) leads to

$$\int_\Omega \mathbb{C}^{-1}\sigma_h:\tau_h\,\mathrm{d}x = -\int_\Omega \tau_h:\gamma_h\,\mathrm{d}x. \tag{4.6}$$

Hence, Eq. (4.5) leads to

$$\begin{aligned}\int_\Omega \operatorname{Curl}\operatorname{Curl}\Phi:\mathbb{C}^{-1}(\sigma-\sigma_h)\,\mathrm{d}x &= \int_\Omega \operatorname{Curl}(\psi-\Psi):(-\gamma_h-\mathbb{C}^{-1}\sigma_h)\,\mathrm{d}x + \int_\Omega \operatorname{Curl}\Psi:(-\gamma_h-\mathbb{C}^{-1}\sigma_h)\,\mathrm{d}x\\ &= -\int_\Omega \operatorname{Curl}(\psi-\Psi):(\gamma_h+\mathbb{C}^{-1}\sigma_h)\,\mathrm{d}x\\ &= \int_\Omega (\psi-\Psi)\cdot\operatorname{curl}_h(\gamma_h+\mathbb{C}^{-1}\sigma_h)\,\mathrm{d}x + \int_{\cup\mathscr{E}_h}(\psi-\Psi)\cdot\big[(\gamma_h+\mathbb{C}^{-1}\sigma_h)t_E\big]\,\mathrm{d}s,\end{aligned} \tag{4.7}$$

(curl_h denotes the $\mathscr{T}_h$-piecewise curl operator). For any $V \in \mathscr{S}^0(\mathscr{T}_h)^2$, i.e., V is $\mathscr{T}_h$-piecewise constant and possibly discontinuous, we compute

$$\begin{aligned}\int_\Omega \varepsilon(v):(\sigma-\sigma_h)\,\mathrm{d}x &= \int_\Omega \varepsilon(v):(\sigma-\sigma_h+\operatorname{As}(\sigma_h))\,\mathrm{d}x = \int_\Omega \nabla v:(\sigma-\sigma_h+\operatorname{As}(\sigma_h))\,\mathrm{d}x\\ &= \int_{\Gamma_N} v(g-\sigma_h n)\,\mathrm{d}s + \int_\Omega \nabla v:\varphi\,\mathrm{d}x - \int_\Omega (v-V)\cdot\operatorname{div}(\sigma-\sigma_h)\,\mathrm{d}x\\ &\leqslant \int_{\Gamma_N} v(g-\sigma_h n)\,\mathrm{d}s - \int_\Omega (v-V)\cdot\operatorname{div}(\sigma-\sigma_h)\,\mathrm{d}x + \|\mathbb{C}^{-1/2}\varphi\|_{2;\Omega}\|\mathbb{C}^{1/2}\nabla v\|_{2;\Omega}.\end{aligned} \tag{4.8}$$

It follows from Korn's inequality that there is a constant c_6 such that

$$\|\mathbb{C}^{1/2}\nabla v\|_{2;\Omega} \leqslant c_6\|\mathbb{C}^{1/2}\varepsilon(v)\|_{2;\Omega}.$$

From Eqs. (4.3), (4.7) and (4.8) (recall that $h_{\mathscr{T}_h}$ resp. $h_{\mathscr{E}_h}$ are mesh-sizes)

$$\begin{aligned}\|\mathbb{C}^{-1/2}(\sigma-\sigma_h)\|_{2;\Omega}^2 \leqslant{}& \|\mathbb{C}^{-1/2}\varphi\|_{2;\Omega}\|\mathbb{C}^{1/2}\nabla v\|_{2;\Omega} + \sqrt{2\mu}\|h_{\mathscr{T}_h}^{-1}(v-V)\|_{2;\Omega}1\Big/\sqrt{2\mu}\|h_{\mathscr{T}_h}\operatorname{div}(\sigma-\sigma_h)\|_{2;\Omega}\\ &+ \sqrt{2\mu}\|h_{\mathscr{E}_h}^{-1/2}(v-\tilde V)\|_{2;\Gamma_N}1\Big/\sqrt{2\mu}\|h_{\mathscr{E}_h}^{1/2}(g-\sigma_h n)\|_{2;\Gamma_N}\\ &+ 1/\sqrt{2\mu}\|h_{\mathscr{T}_h}^{-1}(\psi-\Psi)\|_{2;\Omega}\sqrt{2\mu}\|h_{\mathscr{T}_h}\operatorname{curl}_h(\gamma_h+\mathbb{C}^{-1}\sigma_h)\|_{2;\Omega}\\ &+ 1\Big/\sqrt{2\mu}\|h_{\mathscr{E}_h}^{-1/2}(\psi-\Psi)\|_{2;\bigcup\mathscr{E}_h}\sqrt{2\mu}\|h_{\mathscr{E}_h}^{1/2}[(\gamma_h+\mathbb{C}^{-1}\sigma_h)t_E]\|_{2;\bigcup\mathscr{E}_h}\\ &+ \|\mathbb{C}^{-1/2}\varphi\|_{2;\Omega}\|\mathbb{C}^{-1/2}(\sigma-\sigma_h)\|_{2;\Omega}.\end{aligned} \tag{4.9}$$

By Poincaré's inequality with V being the elementwise integral mean of v, and $\tilde{V}|_E$ the integral mean of $v|_E$ for an edge $E \subseteq \Gamma_N$,

$$\|h_{\mathscr{T}_h}^{-1}(v - V)\|_{2;\Omega} \leqslant c_7 \|\nabla v\|_{2;\Omega} \tag{4.10}$$

is bounded independently of the size of the elements. According to a weak interpolation operator due to Clément (see [5,7,11,16,17] and [13,14] for explicit bounds on c_8 and c_9) one can define Ψ such that

$$\|h_{\mathscr{T}_h}^{-1}(\psi - \Psi)\|_{2;\Omega} + \|h_{\mathscr{E}_h}^{-1/2}(\psi - \Psi)\|_{2;\bigcup \mathscr{E}_h} \leqslant c_8 \|\nabla \psi\|_{2;\Omega} = c_8 \|\operatorname{Curl} \psi\|_{2;\Omega}, \tag{4.11}$$

$$\|h_{\mathscr{E}_h}^{-1/2}(v - \tilde{V})\|_{2;\Gamma_N} \leqslant c_9 \|\nabla v\|_{2;\Omega} \tag{4.12}$$

are bounded independently of the size of the elements. From (4.9)–(4.12), we deduce with Young's inequality, $ab \leqslant a^2/(2c) + b^2 c/2$ for all $a, b, c > 0$,

$$\begin{aligned} \|\mathbb{C}^{-1/2}(\sigma - \sigma_h)\|_{2;\Omega}^2 \leqslant Cc_{10}\Big(&\|\mathbb{C}^{-1/2}\varphi\|_{2;\Omega}^2 + 2\mu \|h_{\mathscr{T}_h} \operatorname{curl}_h(\gamma_h + \mathbb{C}^{-1}\sigma_h)\|_{2;\Omega}^2 + 1/(2\mu)\|h_{\mathscr{E}_h}^{1/2}(g - \sigma_h n)\|_{2;\Gamma_N} \\ &+ 2\mu \|h_{\mathscr{E}_h}^{1/2}[(\gamma_h + \mathbb{C}^{-1}\sigma_h)t_E]\|_{2;\bigcup \mathscr{E}_h}^2 + 1/(2\mu)\|h_{\mathscr{T}_h}(f + \operatorname{div}\sigma_h)\|_{2;\Omega}^2\Big) \\ &+ c_{11}/C\Big(\|\mathbb{C}^{-1/2}\varepsilon(v)\|_{2;\Omega}^2 + \|\mathbb{C}^{-1/2}(\sigma - \sigma_h)\|_{2;\Omega}^2 + \mu/2\|\operatorname{Curl}\psi\|_{2;\Omega}^2\Big) \end{aligned} \tag{4.13}$$

with $C := 2c_{11}c_{12} > 0$ and constants $c_{10}c_{11} > 0$. A closer inspection of $\|\mathbb{C}^{-1/2}\operatorname{Curl}\psi\|_{2;\Omega}$ adopting arguments from [9, p. 199] shows

$$\|\operatorname{Curl}\psi\|_{2;\Omega}^2 \leqslant c_{12} 2\mu \|\mathbb{C}^{-1/2}\operatorname{Curl}\psi\|_{2;\Omega}^2. \tag{4.14}$$

From this, Eq. (4.4) yields the estimate

$$\begin{aligned} c_{13}^{-1}\|\mathbb{C}^{-1/2}(\sigma - \sigma_h)\|_{2;\Omega}^2 \leqslant{}& \|h_{\mathscr{T}_h}\operatorname{curl}_h(\mathbb{C}^{-1}\sigma_h + \gamma_h)\|_{2;\Omega}^2 + \|h_{\mathscr{E}_h}^{1/2}\big[(\mathbb{C}^{-1}\sigma_h + \gamma_h)t_E\big]\|_{2;\mathscr{E}_h^0}^2 \\ &+ \|h_{\mathscr{T}_h}\operatorname{div}(\sigma - \sigma_h)\|_{2;\Omega}^2 + \|\mathbb{C}^{-1/2}\operatorname{As}(\sigma_h)\|_{2;\Omega}^2 + \|h_{\mathscr{E}_h}(g - \sigma_h n)\|_{2;\Gamma_N}^2. \end{aligned} \tag{4.15}$$

This concludes the proof. $\square$

5. Implementation of PEERS

In this section we describe the realization of PEERS. All numerical results in this paper are performed by using a Matlab implementation of PEERS in spirit of Alberty et al. [1]. We emphasize on the stiffness matrices which result in the global linear system of equations $Ax = b$, namely

$$\begin{pmatrix} B & C & D & E & F \\ C^{\mathrm{t}} & 0 & 0 & 0 & 0 \\ D^{\mathrm{t}} & 0 & 0 & 0 & 0 \\ E^{\mathrm{t}} & 0 & 0 & 0 & 0 \\ F^{\mathrm{t}} & 0 & 0 & 0 & 0 \end{pmatrix} \begin{pmatrix} x_\sigma \\ x_u \\ x_\gamma \\ x_{\lambda_E} \\ x_{\lambda_F} \end{pmatrix} = \begin{pmatrix} b_D \\ b_f \\ 0 \\ 0 \\ b_g \end{pmatrix}. \tag{5.1}$$

The symmetric and positive definite matrix B corresponds to the bilinear form a, C and D result from the bilinear form b. The continuity of stress vectors along inner edges is implemented through Lagrangian multipliers in the matrix E for interior edges and F for edges on the Neumann boundary $\overline{\Gamma}_N$. (See [21] for further details.) The components x_σ, x_u, x_γ, x_{λ_E} and x_{λ_F} of the unknown vector x correspond to the basis of Σ_h, $\mathscr{U}_h$, $\mathscr{W}_h$ and to the Lagrange multipliers. The components b_D, b_f and b_g reflect inhomogeneous Dirichlet boundary conditions, the volume force and applied surface forces. To approximate the integrals of the Dirichlet-conditions in the right-hand side a 3-point-Gauß-quadrature is used.

On a triangle $T \in \mathscr{T}_h$ with vertices P_1, P_2, P_3 and center of mass $s := (P_1 + P_2 + P_3)/3$ any discrete stress σ_h in $\hat{\Sigma}_h$,

$$\hat{\Sigma}_h := \{\sigma_h \in L^2(\Omega; M^{2\times 2}) : \ \forall T \in \mathscr{T}_h \ \sigma_h|_T \in RT_0(T) \oplus B_0(T)\},$$

is of the form

$$\sigma_h(x) = p + q \otimes (x - s) + r \otimes \mathrm{Curl}\, b^{\mathrm{t}} = \sum_{j=1}^{8} a_j \eta_j(x) \quad (x \in T).$$

Here $p \in \mathbb{R}^{2\times 2}$ and q, r are coefficient vectors in $\mathbb{R}^2$. The basis $\eta_1, \dots, \eta_8$ we implemented is shown in Table 1. The spaces for the Lagrangian multipliers are defined by

$$M_h = \{\lambda : \lambda|_E \in P_0(E)^2,\ E \subset \partial T,\ T \in \mathscr{T},\ \lambda|_E = 0 \text{ for } E \subset \Gamma_D\},$$
$$N_h = \{\kappa : \kappa|_E \in P_0(E)^2,\ E \subset \Gamma_N,\ \kappa|_E = 0 \text{ for } E \subset \Gamma_D\}.$$

We chose (μ_1, μ_2) as a basis of V_h. The basis functions of M_h and N_h for the Lagrange multipliers equal ζ_1, ζ_2 on the edge E and vanish elsewhere. The basis of the rotations in W_h is defined by v_k, where, for each node z_j, the hat function φ_j is given by

$$\varphi_j(z_k) = \delta_{jk} \quad (k = 1, \dots, \mathrm{card}\,(\mathscr{K})), \tag{5.2}$$

card($\mathscr{K}$) denotes the cardinality of the nodes $\mathscr{K}$. The components of the resulting stiffness matrix B,

$$B_{jk} := \int_T (\mathbb{C}^{-1}\eta_j) : \eta_k \,\mathrm{d}x \quad (j, k = 1, \dots, 8),$$

are shown in

$$B = |T| \begin{pmatrix} 2(\alpha+2\beta) & 0 & 0 & 0 & 0 & 0 & 0 & 0 \\ 0 & 2\alpha & 0 & 0 & 0 & 0 & 0 & 0 \\ 0 & 0 & 2\alpha & 0 & 0 & 0 & 0 & 0 \\ 0 & 0 & 0 & 2\alpha & 0 & 0 & 0 & 0 \\ 0 & 0 & 0 & 0 & B_{55} & B_{56} & 0 & -\frac{\beta}{30} \\ 0 & 0 & 0 & 0 & B_{56} & B_{66} & \frac{\beta}{30} & 0 \\ 0 & 0 & 0 & 0 & 0 & \frac{\beta}{30} & B_{77} & B_{78} \\ 0 & 0 & 0 & 0 & -\frac{\beta}{30} & 0 & B_{78} & B_{88} \end{pmatrix},$$

Table 1
Basis functions

$\hat{\Sigma}_h$	$\eta_1 = \begin{pmatrix} 1 & 0 \\ 0 & 1 \end{pmatrix}$	$\eta_2 = \begin{pmatrix} 1 & 0 \\ 0 & -1 \end{pmatrix}$
	$\eta_3 = \begin{pmatrix} 0 & 1 \\ 1 & 0 \end{pmatrix}$	$\eta_4 = \begin{pmatrix} 0 & -1 \\ 1 & 0 \end{pmatrix}$
	$\eta_5 = \begin{pmatrix} 1 \\ 1 \end{pmatrix} (x-s)^{\mathrm{t}}$	$\eta_6 = \begin{pmatrix} 1 \\ -1 \end{pmatrix} (x-s)^{\mathrm{t}}$
	$\eta_7 = \begin{pmatrix} 1 \\ 1 \end{pmatrix} \mathrm{Curl}\, b^{\mathrm{t}}$	$\eta_8 = \begin{pmatrix} 1 \\ -1 \end{pmatrix} \mathrm{Curl}\, b^{\mathrm{t}}$
$\mathscr{U}_h$	$\mu_1 = \begin{pmatrix} 1 \\ 0 \end{pmatrix}$	$\mu_2 = \begin{pmatrix} 0 \\ 1 \end{pmatrix}$
M_h, N_h	$\zeta_1 = \begin{pmatrix} 1 \\ 0 \end{pmatrix}$	$\zeta_2 = \begin{pmatrix} 0 \\ 1 \end{pmatrix}$
$\mathscr{W}_h$	$v_k = \begin{pmatrix} 0 & \varphi_k \\ -\varphi_k & 0 \end{pmatrix}$	$(k = 1, 2, 3)$

while the remaining coefficients are

$$B_{55} = \frac{\alpha}{6}\sum_{\ell=1}^{3}|P_\ell - s|^2 + \frac{\beta}{12}\sum_{j,k=1}^{2}\sum_{\ell=1}^{3}(P_{\ell j} - s_j)(P_{\ell k} - s_k)^{\mathrm{t}},$$

$$B_{56} = \frac{\beta}{12}\sum_{\ell=1}^{3}((P_{\ell 1} - s_1)^2 - (P_{\ell 2} - s_2)^2),$$

$$B_{66} = \frac{2\alpha + \beta}{12}\sum_{\ell=1}^{3}|P_\ell - s|^2 - \frac{\beta}{6}\sum_{\ell=1}^{3}(P_{\ell 1} - s_1)(P_{\ell 2} - s_2),$$

$$B_{77} = \frac{(2\alpha + \beta)}{180}\left(\sum_{j=1}^{3}\sum_{k=1}^{2}\lambda_{j,k}^2\right) - \frac{\beta}{90}\left(\sum_{j=1}^{3}\lambda_{j,1}\lambda_{j,2}\right),$$

$$B_{78} = \frac{\beta}{180}\left(-\sum_{j=1}^{3}\lambda_{j,1}^2 + \sum_{j=1}^{3}\lambda_{j,2}^2\right),$$

$$B_{88} = \frac{(2\alpha + \beta)}{180}\left(\sum_{j=1}^{3}\sum_{k=1}^{2}\lambda_{j,k}^2\right) + \frac{\beta}{90}\left(\sum_{j=1}^{3}\lambda_{j,1}\lambda_{j,2}\right).$$

(Here, $P_{\ell k}$ ($\ell \in \{1,2,3\}, k \in \{1,2\}$) denotes the kth component of the ℓth vertex of a triangle $T \in \mathcal{T}_h$.)

The bilinear form $b(\eta_i; \mu_j, v_k)$ results into two matrices C and D, with components

$$C_{jk} = \int_T \mu_k \cdot \operatorname{div}\eta_j \,\mathrm{d}x \quad (j = 1,\ldots,8; k = 1,2),$$

$$D_{jk} = \int_T \eta_j : v_k \,\mathrm{d}x \quad (j = 1,\ldots,8; k = 1,2,3).$$

We obtain the local stiffness matrices

$$C = 2|T|\begin{pmatrix} 0 & 0 \\ 0 & 0 \\ 0 & 0 \\ 0 & 0 \\ 1 & 1 \\ 1 & -1 \\ 0 & 0 \\ 0 & 0 \end{pmatrix} \quad \text{and} \quad D = \begin{pmatrix} 0 & 0 & 0 \\ 0 & 0 & 0 \\ 0 & 0 & 0 \\ -\frac{2}{3}|T| & -\frac{2}{3}|T| & -\frac{2}{3}|T| \\ D_{51} & D_{52} & D_{53} \\ D_{61} & D_{62} & D_{63} \\ D_{71} & D_{72} & D_{73} \\ D_{81} & D_{82} & D_{83} \end{pmatrix},$$

where for $j = 1,2,3$

$$D_{5j} = \frac{|T|}{12}(P_{jy} - s_2 - P_{jx} + s_1),$$

$$D_{6j} = \frac{|T|}{12}(P_{jy} - s_2 + P_{jx} - s_1),$$

$$D_{71} = \frac{1}{120}(P_{2y} - P_{3y} + P_{3x} - P_{2x}),$$

$$D_{72} = \frac{1}{120}(P_{3y} - P_{1y} + P_{1x} - P_{3x}),$$

$$D_{73} = \frac{1}{120}(P_{1y} - P_{2y} + P_{2x} - P_{1x}),$$

$$D_{81} = \frac{1}{120}(P_{2y} - P_{3y} - P_{3x} + P_{2x}),$$

$$D_{82} = \frac{1}{120}(P_{3y} - P_{1y} - P_{1x} + P_{3x}),$$

$$D_{83} = \frac{1}{120}(P_{1y} - P_{2y} - P_{2x} + P_{1x}).$$

The Lagrangian multipliers contribute to the matrices E and F, given by

$$E_{jk} = F_{jk} = -\int_E \eta_j \cdot n_E \cdot \zeta_k \, \mathrm{d}s$$

for $j = 1, \ldots, 8, k = 1, 2$ and an edge $E = \mathrm{conv}\{P_1, P_2\} \equiv (E_1, E_2)$. Two neighboring elements T_1, T_2 with common edge E result in two matrices E_{T_1}, E_{T_2}, where

$$E_{T_1} = \begin{pmatrix} -E_2 & -E_2 & E_1 & -E_1 & -\gamma & -\gamma & 0 & 0 \\ E_1 & -E_1 & -E_2 & -E_2 & -\gamma & \gamma & 0 & 0 \end{pmatrix}^t$$

with $\gamma = (E_2, -E_1) \cdot (P_1 - s)$. The matrix E_{T_2} is then computed by $E_{T_2} = -E_{T_1}$ and using the center of mass of the triangle T_2 instead of T_1. For the Lagrangian multipliers corresponding to the Neumann boundary only one matrix F of the form $F = E_{T_1}$ is necessary for every $E \subset \Gamma_N$ and neighboring element T.

6. Numerical examples

We investigate three model problems of two-dimensional plain strain to provide experimental evidence of the robustness, reliability and efficiency of the a posteriori error estimate as the superiority of Algorithm (A) over a uniform mesh-refining.

6.1. L-shaped domain with analytic solution

The first model example on the L-shaped domain shown in Fig. 3 models singularities arising at re-entrant corners. Using polar coordinates (r, θ), $-\pi < \theta \leqslant \pi$, which are centered at the re-entrant corner, the exact solution u with radial component u_r is

$$u_r(r, \theta) = \frac{r^\alpha}{2\mu}(-(\alpha+1)\cos((\alpha+1)\theta) + (C_2 - (\alpha+1))C_1\cos((\alpha-1)\theta)),$$
$$u_\theta(r, \theta) = \frac{r^\alpha}{2\mu}((\alpha+1)\sin((\alpha+1)\theta) + (C_2 + \alpha - 1)C_1\sin((\alpha-1)\theta)).$$

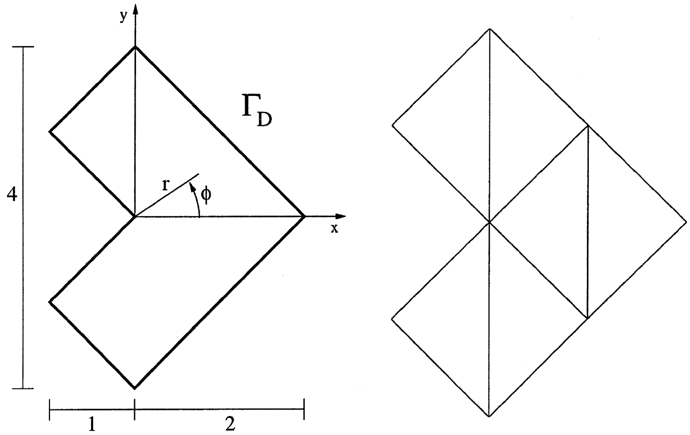

Fig. 3. System and initial mesh in Example 6.1.

The parameters are $C_1 = -\cos((\alpha+1)\omega)/\cos((\alpha-1)\omega)$, $C_2 = 2(\lambda+2\mu)/(\lambda+\mu)$ where $\alpha = 0.54448373\ldots$ is the positive solution of $\alpha\sin 2\omega + \sin 2\omega\alpha = 0$ for $\omega = 3\pi/4$; the Young modulus is $E = 100\,000$ and the Poisson ratio varies in the range $0.3 \leqslant \nu < 1/2$.

The standard FEM for the displacement formulation shows locking as shown Fig. 1 and discussed in Section 1. The PEERS performs much better as shown in Fig. 2 for uniform meshes and in Fig. 2 for automatically generated meshes by Algorithm (A).

In Table 2 the errors and the rates of convergence are displayed for $\nu = 0.3$. For a mesh with N degrees of freedom, $h := \sqrt{N}$ represents an averaged mesh-size and the energy error is $|||\sigma - \sigma_h||| = ||\mathbb{C}^{-1/2}(\sigma - \sigma_h)||2, \Omega$. The experimental convergence rate (CR) is defined as a corresponding (negative) slope in Fig. 2; CR is shown in Table 2 and computed with the entries of the current and the preceding mesh.

We observe that the experimental convergence rate tends to α which is expected theoretically according to approximation results on uniform meshes of singular functions like u. The quotient $|||\sigma - \sigma_h|||/\eta(\sigma;\mathscr{T}_h)$ of the energy norm of the stress error and the a posteriori error bound $\eta(\sigma;\mathscr{T}_h) := (\sum_{T\in\mathscr{T}_h}\eta_T^2)^{1/2}$ is seen to be nicely bounded from above and below. This confirms numerically that the a posteriori error estimate is h-independent.

Table 3 displays the ratio $|||\sigma - \sigma_h|||/\eta(\sigma;\mathscr{T}_h)$ (which gives an estimate for c_3) for different values of $h \to 0$ and $\lambda \to \infty$ in Example 6.1.

In Figs. 2 and 4 and Table 4 we summarize the results of our computations with Algorithm (A). The final mesh after nine adaptive refinements is shown in Fig. 5.

6.2. Cook's membrane problem

As a further test example we investigate a tapered panel clamped on one end and subjected to a shearing load on the opposite end with $f = 0$ and $g(x,y) = (0,1000)$ if $(x,y) \in \Gamma_N$ with $x = 48$ and $g = 0$ on the remaining part of Γ_N as shown in Fig. 6; $E = 1$ and $\nu = 1/3$. The linear elastic version of this simulation is often referred to as Cook's membrane problem, and constitutes a standard test for bending dominated response.

Within eight refinement steps, Algorithm (A) generates a mesh and a stress approximation displayed in Fig. 7.

Fig. 8 shows the vertical displacement of the top right corner vs the number of elements for two series of meshes, namely for a uniform and and an adaptive mesh generated with Algorithm (A). We may conclude that the adaptively refined discretization is more efficient than the uniform one and so the refinement towards the top corner points appears reasonable.

In comparison with the numerical results reported in [6], both adaptive schemes are of equally good performance. The exact solution is unknown to the authors (the value for the exact displacement in Fig. 8 was taken from [6]). To asses the quality of the meshes, we therefore compute the error estimator $\eta(\sigma;\mathscr{T}_h)$ which is displayed in Fig. 9. We observe for uniform and adapted meshes an experimental convergence rate 1 which is independent of the Poisson ratio ν. The adaptive Algorithm (A) is significantly better than a simple uniform discretization.

Table 2
Errors and convergence rates (CR) on uniform meshes in Example 6.1 for $\nu = 0.3$

N	h	$\|\|\|\sigma - \sigma_h\|\|\|$	CR	$\|\|u - u_h\|\|_{2;\Omega}$	CR	$\frac{\|\|\|\sigma-\sigma_h\|\|\|}{\eta(\sigma;\mathscr{T}_h)}$
78	1.4142	0.007686		2.8676e−05		66.3309
317	0.7071	0.006166	0.3142	1.4955e−05	0.9286	69.6894
1281	0.3536	0.004503	0.4501	7.5946e−06	0.9704	72.2536
5153	0.1768	0.003159	0.5094	3.8188e−06	0.9878	72.4184
20 673	0.0884	0.002188	0.5284	1.9140e−06	0.9944	72.3607
82 817	0.0442	0.001508	0.5362	9.5799e−07	0.9974	72.3500

Table 3
Quotients for $v = 0.49999$ for PEERS on uniform mesh in Example 6.1

N	h	$\frac{\|\|\|\sigma-\sigma_h\|\|\|}{\eta(\sigma;\mathscr{T}_h)}$
78	1.4142	94.1275
317	0.7071	79.8191
1281	0.3536	77.9129
5153	0.1768	76.4355
20 673	0.0884	75.9282
82 817	0.0442	75.7658

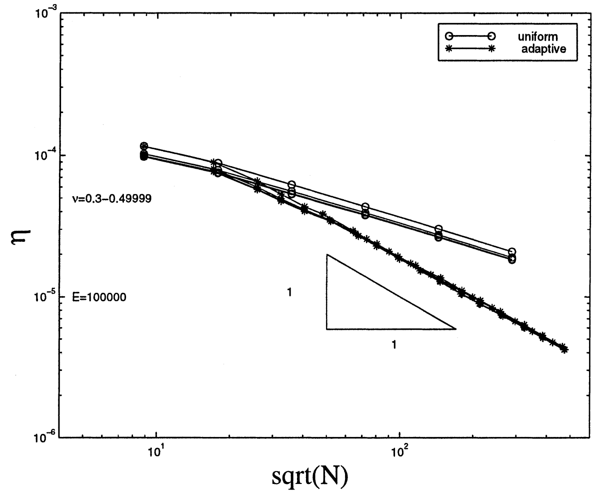

Fig. 4. Error estimator $\eta = \eta(\sigma;\mathscr{T}_h)$ vs mesh-size $\sqrt{N}$ in Example 6.1.

Table 4
Terms of the error estimator for $v = 0.3$ and uniform mesh refinement: $\eta^2_{\mathrm{curl}} := \sum_{T\in\mathscr{T}} h_T^2 \|\mathrm{curl}(\mathbb{C}^{-1}\sigma_h + \gamma_h)\|^2_{2;T}$, $\eta^2_{\mathrm{As}} := \sum_{T\in\mathscr{T}} h_T^2 \frac{1}{\mu^2}\|\mathrm{As}(\sigma_h)\|^2_{2;T}$, $\eta^2_E := \sum_{E\in\mathscr{E}} h_E\Big(\|[(\mathbb{C}^{-1}\sigma_h + \gamma_h)t_E]\|^2_{2;\partial T\setminus\Gamma} + \|[(\mathbb{C}^{-1}\sigma_h + \gamma_h - \nabla u_D)t_E]\|^2_{2;\partial T\cap\Gamma_D} + \|g - \sigma_h n\|^2_{2;\Gamma_N}\Big)$

N	h	η_{curl}	CR	η_{As}	CR	η_E	CR
78	1.4142	3.5342e−05		9.4257e−06		1.0995e−04	
317	0.7071	3.8710e−05	−0.1298	1.3661e−05	−0.5293	7.8386e−05	0.4827
1281	0.3536	2.6029e−05	0.5684	1.0976e−05	0.3134	5.5559e−05	0.4929
5153	0.1768	1.7836e−05	0.5431	7.9072e−06	0.4712	3.9018e−05	0.5078
20 673	0.0884	1.2316e−05	0.5331	5.5175e−06	0.5180	2.7068e−05	0.5265
82 817	0.0442	8.4722e−06	0.5392	3.8165e−06	0.5312	1.8667e−05	0.5355

6.3. Compact tension specimen

A compact tension specimen, shown in Fig. 10, is loaded with a surface load $g = (100, 0)$ on Γ_N (given by $|y| = 60$ mm) and $f = 0$; $E = 100\,000$ and $v = 1/3$. The specimen is subjected to a vertical elongation or compression. As the problem is symmetric, one half of the domain was discretized. We fixed the horizontal displacement with the constraint that the integral mean of all horizontal displacements is 0.

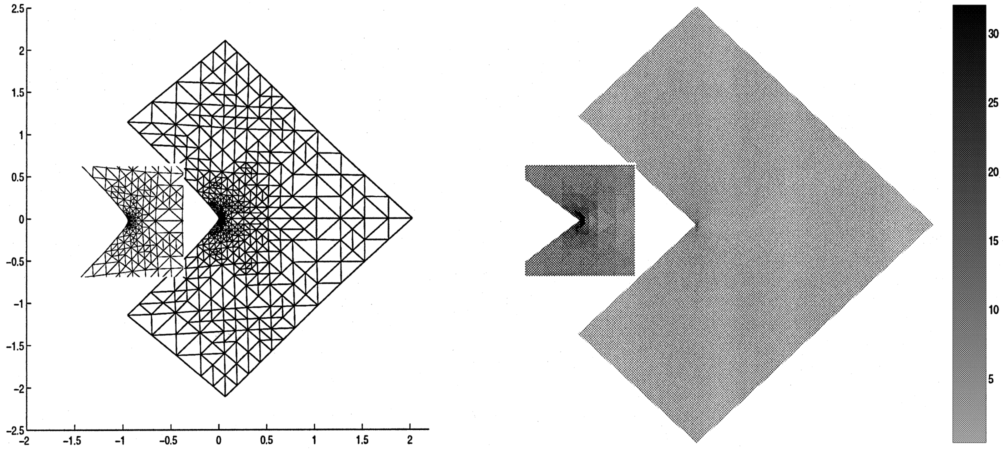

Fig. 5. Deformed mesh (left, displacements magnified by factor 2000) and von-Mises stress (right, with color bar) plus a magnified detail of the neighborhood of the re-entering corner after nine refinements ($N = 12\,174$) with Algorithm (A).

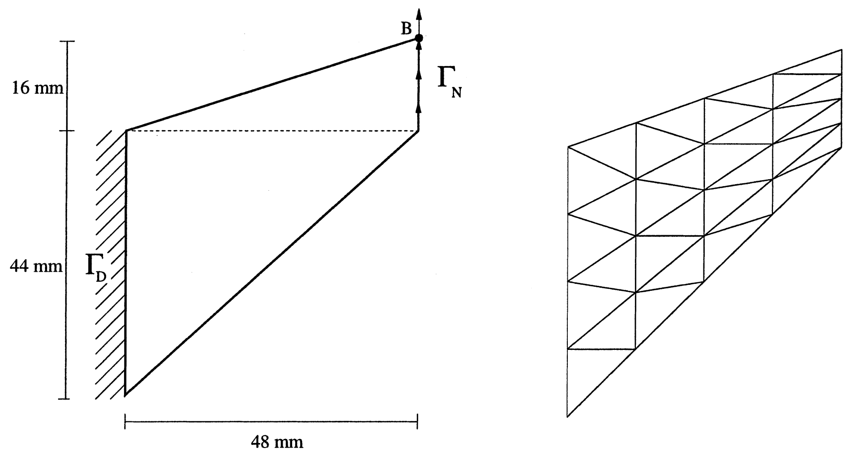

Fig. 6. Cook's membrane problem. System and initial mesh.

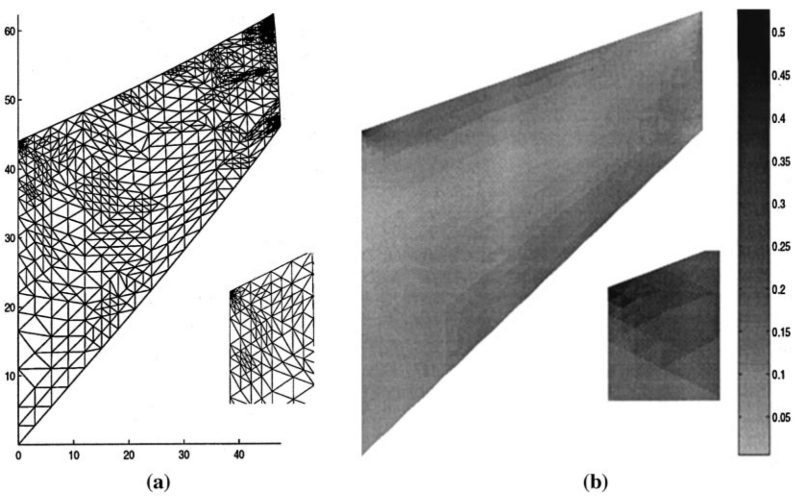

Fig. 7. Deformed mesh (left, displacements magnified by factor 1/10) and von-Mises stress (right, with color bar) plus a magnified detail of the neighborhood of the upper left corner after eight refinements with Algorithm (A) for $E = 1$.

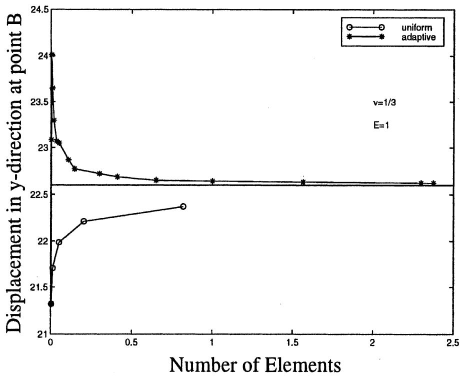

Fig. 8. Vertical displacement of the top corner point B vs number of elements.

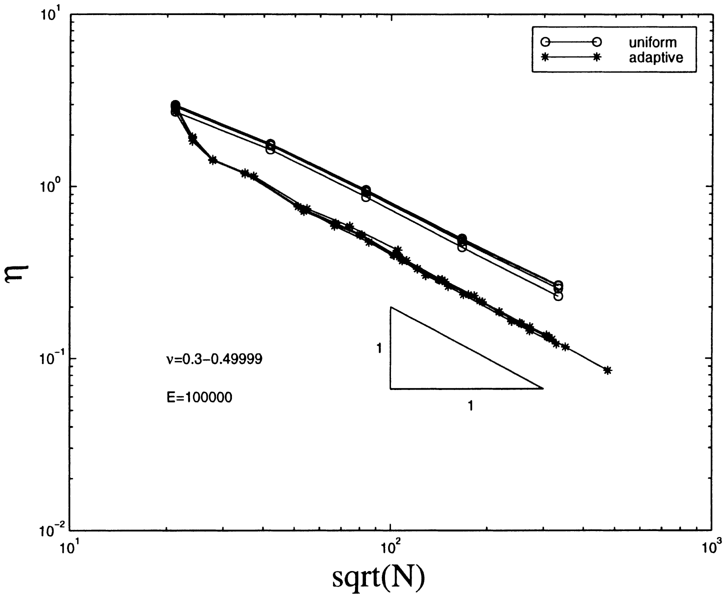

Fig. 9. Error estimator $\eta = \eta(\sigma; \mathscr{T}_h)$ vs mesh-size $\sqrt{N}$ in Example 6.1.

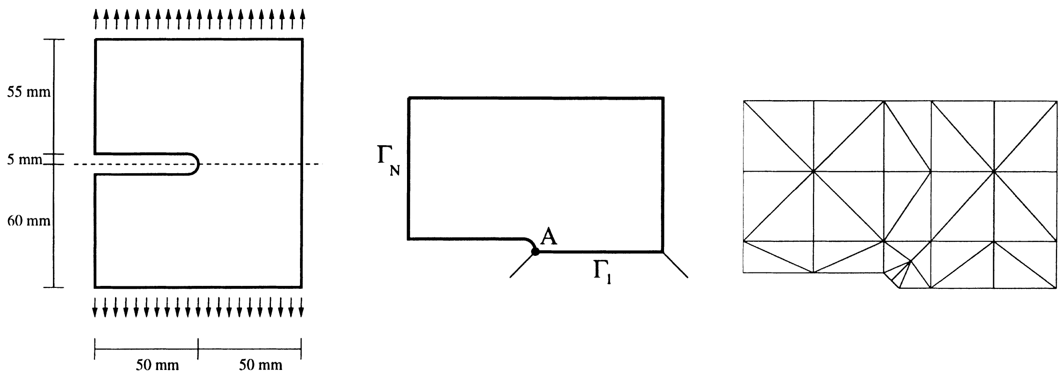

Fig. 10. System and initial mesh in Example 6.3.

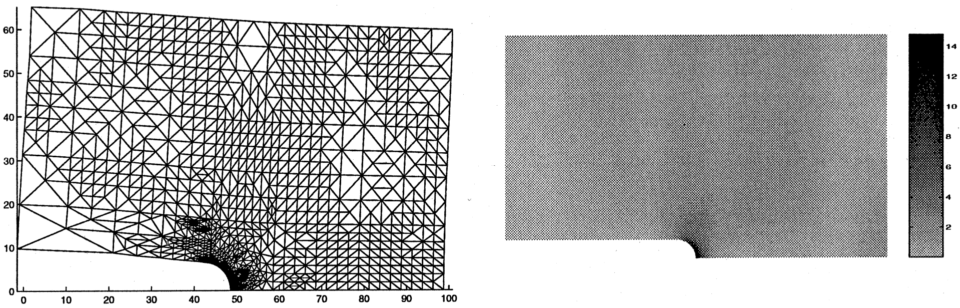

Fig. 11. Deformed mesh (left, displacements magnified by factor 1/100) and von-Mises stress (right, with color bar) after seven refinements with Algorithm (A) for $E = 1$ in Example 6.3.

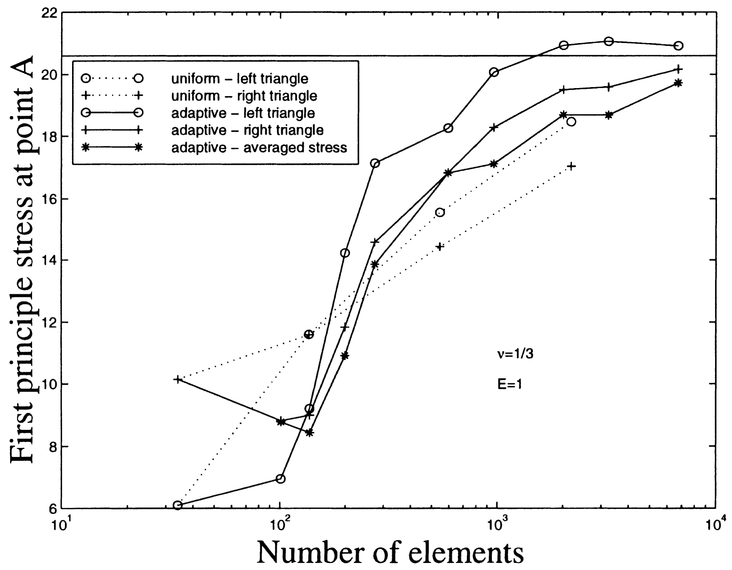

Fig. 12. Principle stress at point A vs number of elements in Example 6.3.

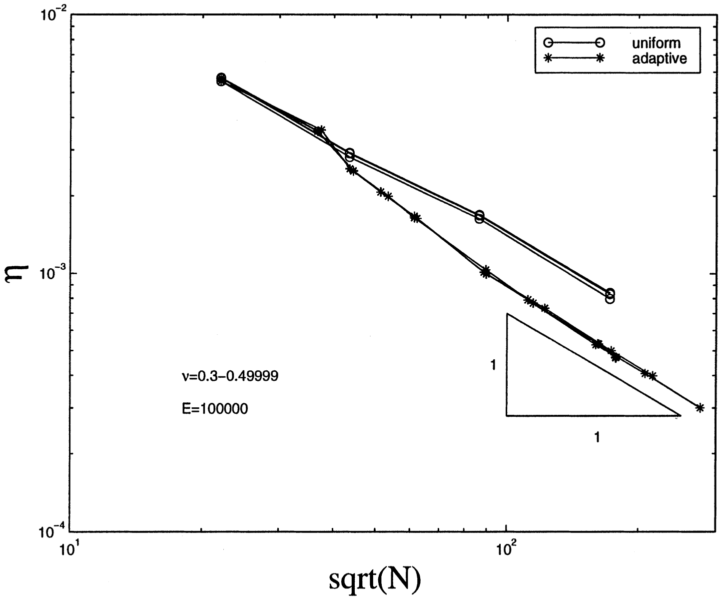

Fig. 13. Error estimator $\eta = \eta(\sigma; \mathscr{T}_h)$ vs mesh-size $\sqrt{N}$ in Example 6.3.

Within seven refinement steps, Algorithm (A) generates a mesh and a stress approximation displayed in Fig. 11. We observe a refinement towards the circular boundary near point A which appears reasonable as we might expect a smoothened singularity there.

As a benchmark, we calculated the principal stress at point A displayed in Fig. 12 (see Fig. 10 for the location of A). Since point A is a node, it is unclear which triangle should contribute to the approximation. Hence, we displayed the values for the two triangles at that point and the approximation obtained by an averaged stress approximation. The adapted discretizations perform much more efficiently than the uniform ones.

To asses the quality of the meshes, we displayed the error estimator η in Fig. 9 for various values of the Poisson ratio. Again, uniform and adapted meshes show an experimental convergence rate 1 independently of the Poisson ratio v. Also, the adaptive Algorithm (A) yields significantly better results than a simple uniform discretization (see Fig. 13).

Acknowledgements

This paper has been initiated while G. Dolzmann visited the Mathematisches Seminar at the Christian-Albrechts-Universität zu Kiel, whose hospitality is gratefully acknowledged. D.S. Helm thanks the Max Planck Institute for Mathematics in the Sciences in Leipzig for two short visits.

References

[1] J. Alberty, C. Carstensen, S.A. Funken, Remarks around 50 lines of Matlab: short finite element implementation, Berichtsreihe des Mathematischen Seminars Kiel, Technical Report 98-11, Christian-Albrechts-Universität zu Kiel, Kiel, 1997, Num. Alg., accepted for publication (http://www.numerik.uni-kiel.de/reports/1998/98-11.html).
[2] A. Alonso, Error estimators for a mixed method, Numer. Math. 74 (1996) 385–395.
[3] D.N. Arnold, F. Brezzi, J. Douglas, PEERS: A new finite element for plane elasticity, Japan J. Appl. Math. 1 (1984) 347–367.
[4] I. Babuška, W.C. Rheinboldt, Error estimates for adaptive finite element computations, SIAM Numer. Anal. 15 (1978) 736–754.
[5] D. Braess, Finite Elements, Cambridge University Press, Cambridge, 1997.
[6] D. Braess, O. Klaas, R. Niekamp, E. Stein, F. Wobschal, Error indicators for mixed finite elements in 2-dimensional linear elasticity, Comput. Methods Appl. Mech. Engrg. 127 (1995) 345–356.
[7] S.C. Brenner, L.R. Scott, The Mathematical Theory of Finite Element Methods, Texts Appl. Math., vol. 15, Springer, New York, 1994.
[8] F. Brezzi, J. Douglas, L.D. Marini, Recent results on mixed finite element methods for second order elliptic problems, in: Vistas in Applied Mathematics. Numerical Analysis, Atmospheric Sciences and Immunology, Springer, Berlin, 1986.
[9] F. Brezzi, M. Fortin, Mixed and Hybrid Finite Element Methods, Springer, Berlin, 1991.
[10] C. Carstensen, A posteriori error estimate for the mixed finite element method, Math. Comp. 66 (1997) 465–476.
[11] C. Carstensen, Weighted Clément-type interpolation and a posteriori analysis for FEM, Berichtsreihe des Mathematischen Seminars Kiel, Technical Report, 97-19, Christian-Albrechts-Universität zu Kiel, Kiel, 1997, M^2AN, accepted for publication (http://www.numerik.uni-kiel.de/reports/1997/97-19.html).
[12] C. Carstensen, G. Dolzmann, A posteriori error estimates for the mixed FEM in elasticity, Numer. Math. 81 (1998) 187–209.
[13] C. Carstensen, S.A. Funken, Constants in Clément-interpolation error and residual based a posteriori error estimates in finite element methods, Berichtsreihe des Mathematischen Seminars Kiel, Technical Report, 97-11, Christian-Albrechts-Universität zu Kiel, Kiel, 1997, (http://www.numerik.uni-kiel.de/reports/1997/97-11.html).
[14] C. Carstensen, S.A. Funken, Fully reliable localised error control in the FEM, Berichtsreihe des Mathematischen Seminars Kiel, Technical Report, 97-12, Christian-Albrechts-Universität zu Kiel, Kiel, 1997, SIAM J. Sci. Comput., accepted for publication (http://www.numerik.uni-kiel.de/reports/1997/97-12.html).
[15] C. Carstensen, R. Verfürth, Edge residuals dominate a posteriori error estimates for low order finite element methods, Berichtsreihe des Mathematischen Seminars Kiel, Technical Report, 97-6, Christian-Albrechts-Universität zu Kiel, Kiel, 1997, SIAM J. Numer. Anal., accepted for publication (http://www.numerik.uni-kiel.de/reports/1997/97-6.html).
[16] P. Clément, Approximation by finite element functions using local regularization, RAIRO Sér. Rouge Anal. Numér. R-2 (1975) 77–84.
[17] P.G. Ciarlet, The Finite Element Method for Elliptic Problems, North-Holland, Amsterdam, 1978.
[18] K. Eriksson, D. Estep, P. Hansbo, C. Johnson, Introduction to adaptive methods for differential equations, Acta Numerica (1995) 105–158.
[19] B.X. Fraeijs de Veubeke, Stress function appoach, in: Proceedings of the World Congress on the Finite Element Method in Structural Mechanics, Bournemouth, 1975.

[20] V. Girault, P.A. Raviart, Finite Element Methods for Navier–Stokes Equations, Springer, Berlin, 1986.
[21] R. Stenberg, A family of mixed finite elements for the elasticity problem, Numer. Math. 53 (1988) 513–538.
[22] R. Temam, Theory and Numerical Analysis of the Navier–Stokes Equations, North-Holland, Amsterdam, 1977.
[23] R. Verfürth, A review of a posteriori error estimation and adaptive mesh-refinement techniques. Wiley-Teubner, 1996.